Downward Continuation of Wide-Angle Seismic data: implications for traveltime tomography uncertainty

C. E. Jimenez-Tejero *[1], M. Prada[1], L. Gomez de la Peña[1], C. R. Ranero[1,2], and V. Sallares[1]

[1]ICM-CSIC, Consejo Superior de Investigaciones Científicas, Instituto de Ciencias del Mar, Barcelona Center for Subsurface Imaging, 08003 Barcelona, Spain
[2] ICREA-Institució Catalana de Recerca i Estudis Avançats, 08010, Barcelona, Spain

Abstract

Controlled-source marine seismic experiments are key in advancing our understanding of the Earth's subsurface structure to study tectonic, magmatic, sedimentary and fluid flow processes. Joint acquisition of Wide-Angle Seismic (WAS) and Multi-Channel Seismic (MCS) streamer data stands as the most robust approach for marine exploration, however effectively mapping subsurface structure remains challenging. The lack of identifiable refractions as first arrivals at short offsets in WAS data leads to illumination gaps of the upper 2-4 km of the subsurface structure at 8-12 km offsets around Ocean Bottom Seismometers (OBS). This inadequate ray coverage at the shallow subsurface limits the performance of Travel Time Tomography (TTT) techniques and affects velocity determination in the sedimentary layer and reflector location, propagating errors to deeper layers.

This study integrates Downward Continuation (DC) to WAS data. Similarly to DC applied to MCS data, redatuming WAS data involves using the acoustic wave equation backward in time. This process virtually repositions the sources to the seafloor, revealing previously masked near-seafloor refractions as first arrivals. This transformation significantly enhances ray coverage in the shallow subsurface, leading to more accurate determinations of both seismic velocity and reflector geometry. By bridging theoretical concepts with a real data application, this study demonstrates the optimization of field seismic data for improved TTT results. This methodology is particularly beneficial for deep water exploration where spatially coincident WAS and MCS are jointly inverted. In such scenarios, DC-processed WAS data provides the refracted phases key for velocity determinations, and that are typically not present in MCS data due to insufficient streamer length relative to the water column depth. Additionally, we contribute to the community by releasing our open-source, High-Performance Computing (HPC) software for WAS data redatuming.

1 Introduction

Estimation of subsurface properties, including P- and S-wave velocities, density and anisotropy, is a crucial issue in geophysics. P-wave velocity (V_p) emerges as a fundamental parameter, aiding in rock type identification and evaluating properties such as porosity, fracturing degree, fluid content and pressure (Arnulf et al. 2021, Reilly et al. 2019, Prada et al. 2019). V_p information is also fundamental in advanced seismic imaging like pre-stack depth migration, where accurate V_p models are critical for achieving detailed images of the subsurface. The creation of accurate V_p models depends on the availability of field data

*ejimenez@icm.csic.es

and of appropriate methodologies such as travel time and waveform tomography. Yet, the full potential of available field data is frequently undervalued.

In marine settings, seismic exploration with controlled source is key to determine the subsurface structure. Seismic velocity is typically obtained through the analysis of the seismic wavefield and the corresponding seismic phases – both reflected and refracted. Marine multichannel seismic (MCS) streamer data provides comparatively high-resolution subsurface information. However, its capacity to retrieve accurate V_p information is significantly affected by streamer length respect to target depth, particularly restricting the capture of refractions (Jimenez-Tejero et al. 2022). This limitation impacts both ray coverage and the maximum depth of reliable velocity determination. WAS data complement MCS records mapping with refracted phases comparatively deeper subsurface structures, mitigating offset limitations to estimate velocity. However, WAS data are typically acquired with a limited amount of Ocean Bottom Seismometers or Hydrophones (OBS/OBH), which in crustal-scale seismic experiments are typically spaced 5-20 km. This receiver spacing results in refracted ray-coverage gaps in the shallow subsurface. In contrast, MCS provides higher coverage with receivers typically spaced as close as 6.25 meters. Consequently, combining information (travel-time or waveform) from MCS and WAS data allows to enhance ray coverage at all depth levels, increasing resolution and reducing uncertainties in tomographic results, and mitigating ambiguous geological interpretations.

In experiments using only MCS data, the offset and consequently the amount of refractions are constrained by the ratio of streamer length to water depth and the subsurface P-wave velocity structure (Jimenez-Tejero et
In such scenarios, the application of redatuming techniques allows transforming the data, so that the availability of refractions can be maximised. Redatuming MCS data involves shifting the source and receiver positions to the seafloor. This transformation enables secondary refractions, initially masked in the original shot gather to emerge as first arrivals in the new virtual gather. Inverting redatumed first arrivals through travel-time tomography leads to an increased ray coverage in the shallow part of the model, thereby providing better constrained velocity models (Gras et al. 2019, Jimenez-Tejero et al. 2022, Prada et al. 2023).

Redatuming techniques encompass both model-driven and data-driven approaches. Model-driven techniques, such as wave equation datuming (WED) (Berryhill 1979, Berryhill 1984, Shtivelman and Caning 1988, Bevc 1997, Mo 1997), rely on extrapolation operators derived from the wave equation. On the other hand, data-driven methods, like cross-correlation redatuming, involve extracting operators directly from input data sets (Berkhout 1997a, Berkhout 1997b). Both approaches use various extrapolation methods, including Kirchhoff summation, plane-wave methods, and finite difference techniques (Berkhout 1981, Gazdag 1978, Arnulf et al. 2011, Cho et al. 2016, Gras et al. 2019, Jimenez-Tejero et al. 2022). While all techniques aim to simulate data acquired at a different surface by applying time shifts and amplitude factors, they vary in their reliance on simplifying assumptions, treatment of wave propagation phenomena, and handling of lateral velocity variations.

Just as with MCS data, challenges regarding masked secondary refractions also arise when dealing with WAS data. However, compared to the more extended use of redatuming in MCS cases, the application to WAS data remains relatively infrequent. Existing studies use redatuming of WAS data, such as wave equation datuming and wavefield extrapolation and decimation for seismic imaging (Barison et al. 2011, Giustiniani et al. 2022) and to extract V_s information from teleseismic arrivals (Zheng et al. 2019).

Building upon our redatuming approach on MCS data through Downward Continuation (DC)(Jimenez-Tejero et a
this study expands the application of DC to marine WAS data recorded on OBS/H. We first explore redatuming using a synthetic benchmark model. Then, we apply DC to WAS field data and conduct a comparative analysis of travel-time tomography results, including joint MCS+WAS. The primary objective remains the reduction of velocity and depth uncertainties within tomographic models, with a particular focus on the sediment layer overlaying higher-velocity basement.

2 Materials and methods

The redatuming of WAS data via DC offers a straightforward implementation, encompassing all data without the necessity for prior phase selection. It is adaptable to irregular new datum surfaces, remains stable in steeply dipping areas, and can accommodate arbitrary V_p models. Despite these advantages, limitations are associated primarily with the finite-difference scheme and the model-dependent nature of redatuming. However, insights from DC applied to MCS data (Jimenez-Tejero et al. 2022) show that the lack of detailed velocity model information does not compromise reliability. Since propagation occurs within the water column with negligible velocity variations, employing a homogeneous yet realistic water velocity value consistently results in errors of less than 2%, compared to using water velocity models derived from field data.

In this section, we first outline the main components of the DC method, which involves solving the two-way acoustic wave equation in a 2D domain, implemented backward in time. We use benchmark synthetic homogeneous V_p models to demonstrate the impact of water column depth, as well as the near-seafloor velocity model, on the registration of refractions in WAS field data experiments. Furthermore, we discuss the main computational aspects of the DC-WAS code that we provide, and describe the data pre-processing techniques employed to enhance the quality of the results. Lastly, we describe the main aspects of the travel-time tomography method used in the analysis.

2.1 Downward Continuation using the 2D Acoustic Wave Propagation

The tool for redatuming seismic data to the seafloor is based on the acoustic wave equation through the water layer, incorporating homogeneous, isotropic, and acoustic approximations. Solving the wave propagation equation entails a finite difference scheme of 6th order in space and 2nd order in time. To prevent artificial numerical reflections, a free surface is applied at the top, coupled with a Convolutional Perfectly Matched Layers (CPML) scheme (Pasalic and McGarry 2010) at the left, right, and bottom boundaries. The wave equation is defined differently outside and inside the PML layers. The acoustic wavefield propagation, represented as $p(r,t)$, for a given source, $f_s(S,t)$, within a velocity model, $v(r,t)$, is expressed as follows:

$$\frac{1}{v^2}\partial_t^2 p = \partial_k^2 p_k + f_\mathrm{s} + f_p^{\mathrm{PML}} \ , \tag{1}$$

$$f_p^{\mathrm{PML}} = \begin{cases} \partial_k \cdot \psi_k(p) + \xi_k(p), \ \mathbf{r} \in \mathrm{PML} \\ \\ 0, \ \mathbf{r} \notin \mathrm{PML} \end{cases} \tag{2}$$

The additional term for the PML layer, denoted as f_p^{PML} is characterized with the auxiliary variables $\psi_k(p)$ and $\xi_k(p)$, governing the evolution for each component (k=x,z) and time step, n, as follows:

$$[\psi_k(p)]^n = a_k \cdot [\psi_k(p)]^{n-1} + b_k \cdot [\partial_k p_k]^n \ , \tag{3}$$

$$[\xi_k(p)]^n = a_k \cdot [\xi_k(p)]^{n-1} + b_k \cdot \left[\partial_k^2 p_k + \partial_k \psi_k(p)\right]^n \ , \tag{4}$$

$$\tag{5}$$

where the parameters a_k and b_k are:

$$a_k = e^{-(\sigma_k+\alpha_k)\cdot\Delta t} \quad , \quad b_k = \frac{\sigma_k}{\sigma_k+\alpha_k}\cdot(a_k-1) \ . \tag{6}$$

with Δt being the time step, σ_k the absorption damping factor of the acoustic wave and α_k the real positive pole shifting factor (Zhang and Shen 2010).

The redatuming of WAS data is performed in a single step. For each OBS gather, the sources are propagated as a supershot backward in time, ensuring accurate waveform transformation. In this process, while the positions of the sources within each OBS gather maintain their original horizontal coordinates, their vertical locations are adjusted to conform to the seafloor bathymetry. The primary objective of redatuming WAS data is to facilitate a clear visualization of near-offset refracted P-waves as first arrivals, which would otherwise be obscured as secondary arrivals. As shown for MCS data (Jimenez-Tejero et al. 2022), the length of recorded refractions is mainly governed by two key parameters: the velocity structure of the subsurface and the depth of the seafloor. The minimum offset with visible refractions as first arrivals in a OBS gather at any marine setting (Jimenez-Tejero et al. 2022), is:

$$\text{Offset}_{\text{min}}^{\text{OBS}} = \begin{cases} \frac{D_s \cdot \left(\frac{u}{w} - \tan\phi\right)}{1+\tan^2\phi} & \text{if } D_s < D_r,\ (\phi > 0) \\ \frac{D_s \cdot \left(\frac{u}{w} + \tan\phi\right)}{1+\tan^2\phi} & \text{if } D_s > D_r,\ (\phi > 0) \\ D \cdot \frac{u}{w} & \text{if } D = D_s = D_r,\ (\phi = 0) \end{cases} \tag{7}$$

where D_s and D_r are the source and receiver depths, the angle ϕ is the seafloor slope, $w = \sqrt{1-u^2}$ and $u = V_{\text{water}}/V_{\text{Earth}}$. We represent Equation 7 for a flat seafloor (ϕ=0) in Fig. 1, exploring the parameter space using benchmark models. All models maintain a constant water velocity of V_{water} = 1.5 km/s and consist of a single homogeneous subsurface layer. The y-axis indicates variations in water column depth, while the x-axis corresponds to the subsurface V_p layer. Consistent with findings from the study on MCS data (Jimenez-Tejero et al. 2022), we observe a decrease in refractions inversely proportional to increasing water depth. Moreover, higher sub-seafloor velocities result in refractions recorded as first arrivals appearing at shorter offsets.

2.2 DC-WAS code: computational and numerical aspects

We present a new software tool for redatuming WAS data using the DC method, written in modern Fortran and tailored for high-performance computing (HPC) environments using Open MPI for efficient parallelization. This section details the computational features of the code, inheriting many aspects from the equivalent software designed for MCS data redatuming (Jimenez-Tejero et al. 2022):

HPC Architecture and Computational Resources MPI parallelization accounts for the number of OBSs to be redatumed. Each set of shots recorded at each OBS gather is downward continued to the seafloor and propagated as a super shot through the water layer back in time. This process is independent for each OBS gather, so the number of OBS gathers is parallelized with the available process slots, i.e. CPUs or cores depending on the operating system. The most efficient performance is achieved when the code is parallelized using the same number of processes as OBS gathers. In this configuration, the computing time ranges from a few seconds to a few minutes. Regarding memory space/RAM consumption, the code is efficient and low-demanding.

WAS data The WAS input field data is directly read in SU format, which is a modification of the standard binary SEG-Y format designed to work with Seismic Unix software (SU). In the SU format, each gather consists of a collection of traces, each attached to a 240-byte header encoding experimental information. Parameters like the common receiver gather location and the offset at each trace can be provided through the headers. The bathymetry is provided as a text file, and the values of the main acquisition parameters (number of receivers, nt, dt, etc) are read from a text file. The OBS gather redatumed results are also stored in SU format.

Data pre-processing Field data processing before redatuming is essential for maximizing the quality of the results. Here, we list some useful processing techniques. OBS gathers, used as input for this software, require two types of muting to avoid noise. It is recommended to truncate the recording time just above the first multiple - the primary reflection of the seismic wave at the sea surface. In a OBS gather for the zero-offset trace, the cut-off at the first multiple is located at $3D_{water}/v_{water}$, where D_{water} refers to the depth of the water column layer. Another type of muting facilitates obtaining cleaner results by eliminating information from the trace before the first arrival. Both muting procedures can be implemented through various forms of filtering or surgical muting. Also, filters such as the Butterworth type can be applied to eliminate frequencies below 2 Hz and above 80 Hz to amplify the signal-to-noise ratio.

2.3 Joint refraction and reflection travel-time tomography

We use a modified version of the code tomo2d (Begovic et al. 2017), originally developed by (Korenaga et al. 2000), to perform the joint refraction and reflection travel-time tomography (Melendez et al. 2015a, Melendez et al. 2015b, Merino et al. 2021). This modified version integrates source and receiver geometry of streamer MCS and WAS data for their joint inversion. The tomographic method computes synthetic travel times with a ray-tracing algorithm based on the graph and ray-bending refinement methods (Moser 1991, Moser et al. 1992). The regularized inversion is performed using a least-square sparse matrix solver, updating the initial model iteratively to minimize the misfit between observed and synthetic travel times. This iterative process continues until a given Chi2 criterion, where the misfit is within the range of travel time picking uncertainty, is satisfied.

3 Results

In this section, we emphasize the advantages of redatuming WAS data to the seafloor, particularly when jointly inverting WAS and MCS travel times. We present the velocity model results obtained through travel time tomography, using MCS data alone and in combination with WAS data for our field data case.

3.1 Synthetic data example

As an initial step, we use a synthetic 1D-gradient model to showcase the advantages of redatuming WAS data to the seafloor, illustrating its potential to improve the resolution of tomographic models, particularly in the few km beneath the seafloor. The example presented in Fig. 2 compares synthetic first arrival travel times of a synthetic OBS gather generated with two different models with the same vertical velocity structure but different water depths. Fig. 2a illustrates the ray path obtained through the shallow-water case with a seafloor depth of 0.5 km, while Fig. 2b represents the deep case with a water depth of 5 km. In Fig. 2c, both synthetic first arrival travel times from each scenario are compared, showing the first arrivals from simulated OBS gathers. Notably, in the shallow-water case (Fig. 2a), the direct water wave extents to approximately 2.5 km of offset, while in the deep-water case (Fig. 2b), it extends to at least 7 km of offset. As evidenced by the ray tracing in Fig. 2b, the segments where the first arrival corresponds to the direct wave, refractions are masked at offsets > 4 km.

Fig. 3a displays complete OBS record of the OBS at 5 km-depth, accompanied by the corresponding ray tracing simulation (Fig. 3c). The panels on the right display the results of the OBS gather redatumed to the seafloor (Fig. 3b) after applying DC. In this new virtual configuration all first arrivals correspond to P-waves refracted through the subsurface. As illustrated by the ray tracing in (Fig. 3d), the DC process significantly increases ray coverage in the shallow layers compared to the original OBS gather (Fig. 3c).

3.2 Field data case

We present a field data case using the 100 km-long line ATLANTIS-I, acquired during the ATLANTIS survey in 2022, southwest of Madeira Island, within the Atlantic Ocean at 31°N (Fig. 4). The dataset comprises MCS data acquired with a 3-km-long streamer and WAS data acquired with 11 OBH spaced 7-8 km apart. Fig. 5 presents the OBH number 4 from the seismic line (Fig. 5a) with its downward continuation to the seafloor (Fig. 5c). Fig. 5-b and -d, provide a closer zoom, highlighting the first arrival picks. Pre-processing for cleaner results for redatuming of the field data includes muting the signal up to the first arrival and from the first multiple (we refer to Figure S1 in the Supplementary Material, which shows the first seven OBH gathers, which are the ones redatumed for this study).

Our primary objective is to employ a joint strategy, combining MCS and WAS data, to estimate the V_p model using TTT. When considering the implementation of the joint strategy for redatuming purposes, it must be noted that the presence of refractions in MCS data is limited by the streamer length, water depth, and subseafloor velocity. In this experiment, the 3-km-long streamer is too short to contain refracted arrivals given the $>$ 4500 m water depth (Jimenez-Tejero et al. 2022). Thus, redatuming the OBS data offers a solution to increase ray coverage, leading to improved accuracy and resolution of the V_p model in the upper 2-3 kilometers.

The results are presented in Fig. 6, Fig. 7 and Fig. 8. To evaluate the use of redatumed WAS data in TTT, we invert for the sediment layer velocity structure and the geometry of the Top of the Basement (TOB) with three different strategies. Initially, we explore a strategy relying solely on travel times from MCS data, used in experiments when no OBS data are available (Fig.6). In the second test, we implement the MCS + WAS joint strategy using the original streamer and OBH records (Fig.7). Finally, in the third test, we extend the joint strategy by inverting WAS data redatumed to the seafloor, defined as MCS+WAS(DC) (Fig. 8).

In each of the three cases, we performed TTT following a Monte Carlo approach to compare the effectiveness of each case in reducing model parameter uncertainty (i.e. velocity and geometry of reflector). The Monte Carlo statistical analysis involves the inversion of 500 realizations. Each of them combines a randomly generated 1D velocity profile as starting model, a set of travel times with Gaussian noise added randomly based on manual picking uncertainty (from 20 to 40 ms), and a randomly generated flat-geometry initial reflector for the TOB. After inverting the 500 realizations, in each case, we compute the improvement factor, $(\sigma_0\text{-}\sigma_f)/\sigma_0)$, which quantifies the reduction in the initial standard deviation of V_p. With respect to the different panels shown in Figs. 6 to 8, the panel a) presents the results of the average V_p velocity model of the 500 realizations, while panel b) illustrates the V_p difference between the initial and final (average) models, and panel c) shows the improvement factor. We refer to the Supplementary Material to visualize the initial V_p model and standard deviation (Fig. S2).

We clarify than in Fig. 8, the redatumed OBH gathers range from 1 to 7. OBH gathers from 8 to 11 were not redatumed because they already present a sufficient number of refractions recorded as first arrivals in their natural configuration, resulting in low standard deviations, as shown in Fig. 7-c). However, it's important to note that all OBH gathers in the same line could be systematically redatumed if desired.

4 Discussion

4.1 Discussion of results

Results show that TTT using only reflections on MCS data provides an apparent well constrained reflector inversion (Fig. 6). However, Fig. 6-b shows that the V_p model is similar to the initial model and that there is little reduction in standard deviation after the 500 realisations (Fig. 6c), indicating that the real V_p is poorly recovered. Even though the geometry of the reflector seems to converge towards a common solution, the final solution departs little from the initial models, with only a marginal reduction of the initial V_p standard deviation.

In contrast, when employing the joint MCS+WAS strategy, the outcomes improves (Fig. 7). Notably,

from OBH number 4 to number 11, there is an increase in V_p differences, and an improvement in the initial deviation occurs from OBH number 8 to 11 (Fig. 7-bc). This improvement occurs in areas with comparatively increased number of refractions which can be identified in the field-geometry OBH sections (Fig.S1 in the Supplementary Material). In contrast, from OBH 1 to 8, the initial deviation barely improves due to a tradeoff between the number of reflections from MCS and the limited number of refractions from WAS data, rendering the V_p model unreliable (Fig. 7-c). Additionally, the joint MCS+WAS inversion exhibits increased uncertainty in the location of the inverted reflector compared to the scenario using only MCS reflections. This result shows that the limited sedimentary refracted P-wave traveltimes from OBS with no DC are not sufficient to converge into a common tomographic solution in terms of velocity structure. This emphasizes the need for increasing refracted traveltime information to outweighs the tomographic information provided by reflected traveltimes that suffer from large velocity-depth trade-off.

When applying the joint strategy with WAS data redatumed to the seafloor, MCS+WAS(DC), the comparison of the initial and final models (Fig. 8-b) reveals consistent reduction in the initial standard deviation (Fig. 8-c) across the entire model. This suggests that the inversion converges towards a single, improved solution regardless of the initial model chosen.

Fig. 9 compares the results obtained using the three different inversion strategies at kilometers 20, 50, and 80 along the seismic line. At kilometers 20 and 50, the reflector depth is similar, while at kilometer 80 it is significantly deeper. Areas with a deeper TOB reflector naturally exhibit more refractions in the raw OBH data (Fig. S1 in the Supplementary Material). Consequently, the joint MCS+WAS strategy performs reasonably well at these locations (Fig. 7). However, the joint strategy with MCS+WAS(DC) further improves the results by reducing uncertainty (Fig. 8). Overall, incorporating first arrivals through the DC redatuming strategy leads to consistently lower parameter uncertainty throughout the model. The V_p model uncertainty remains within a range of 100-150 m/s, and the reflector location uncertainty is constrained to 100 m.

Robust resolution of the velocity structure of the upper few subseafloor km is crucial for understanding processes ranging from oceanic crust formation, e.g. (Arnulf et al. 2011, Grevemeyer et al 2018, Peirce and Hobbs 2
or the interplay between faulting, lithology and fluids, e.g. (Olsen et al. 2020, Arnulf et al. 2021). Most of these settings are located in deep water environments. Our results illustrate the potential to increase the data for available resolving velocities with limited travel time information, particularly in these deep water regions. The inversion of limited refracted travel times may provide velocities and geometries of reflectors biased by the initial assumption (Fig. 9). However, the implementation of DC and joint inversion strategies may mitigate this issue, reducing velocity and geometry uncertainty inherent to TTT , facilitating a more robust assessment of the shallow V_p structure, even if the receiver spacing is large.

The robust constraint provided by shallow velocity structures is essential not only for studies investigating shallow layers but also for deeper crustal-scale studies including the petrological nature of the basement of the crust, e.g. (Grevemeyer et al 2018, Merino et al. 2021) or the tectonic structure of subduction zones (Sallares et al 2021). The joint TTT strategy presented here helps minimize uncertainties related to shallow vertical velocity gradients and the position of the TOB (Figs. 9 and 10). This, in turn, should prevent the propagation of errors to deeper geological layers. This allows for an improved characterization of vertical velocity gradient of the crystalline crust, reducing uncertainties in the petrological interpretation and the location of deeper interfaces (crust-mantle boundary or subduction interplate plate boundary).

4.2 Applications beyond TTT velocity models

Full Waveform Inversion (FWI). The benefits of DC redatuming extend beyond improving TTT imaging. In high-resolution techniques like FWI, where success depends on the quality of the initial model to avoid non-linear challenges like cycle-skipping, incorporating DC within the TTT framework can further enhance these TTT-derived initial models. This significantly improves the probability of FWI converging towards an accurate, high-resolution representation of the subsurface (Gras et al. 2019).

Pre-Stack Depth Migration (PSDM). Although DC redatuming offers valuable advantages in jointly inverting MCS and WAS(DC) data to produce more accurate velocity models with reduced uncertainty in reflector location, caution is necessary before applying these models to tasks like PSDM calculation. Due to the presence of anisotropy in the sediments, seismic waves travel at different velocities depending on the propagation direction, commonly exhibiting faster velocities for the horizontal waves. This results in slower apparent velocities being registered in streamer data from MCS surveys compared to WAS data, where each OBS captures rays traveling longer horizontal distances. In our field data case, the presence of significant anisotropy and the short length (3 km) of the MCS streamer prevent the velocity model obtained with DC-enhanced joint data from achieving an adequate collapse of the shallow part or sediments in the PSDM calculation. Fig. 11 illustrates this issue, where Fig. 11-a shows the difference between velocity models from MCS+WAS(DC) joint inversion and MCS data alone in the shallow section with an average of 18% difference, highlighting significant anisotropy, in which MCS+WAS(DC) model shows faster V_p than MCS model, as expected for a marine sedimentary basins formed by sub-horizontal layers. As expected, using the MCS+WAS(DC) velocity model for PSDM calculation results in a poor collapse in depth of the sediments up to the TOB (Fig. 11-c). Therefore, for PSDM construction in this scenario, a combined model is recommended (Bartolome et al. 2004). This approach utilizes the velocity model derived from MCS data for the shallow section until the TOB and the tomographic model obtained from sub-basement OBS traveltimes for the deeper section (Fig. 11-b).

5 Conclusion

This work focus into the challenge of extracting valuable near-seafloor refraction information often hidden within WAS data, specially in deepwater marine environments. We provide a user-friendly DC software for processing WAS data, adaptable for both local systems and high-performance computing clusters. Using modern Fortran and open MPI optimization, our tool efficiently handles OBS/OBH records in Seismic Unix (SU) format.

- The core of the approach lies in the DC algorithm, applied to each OBS/OBH record using the 2D acoustic solver, leading to the relocation of sources to the seafloor. This process unmasks hidden secondary refractions, enhancing their identification as first arrivals in the new virtual configuration.

- Our analysis highlights the power of joint TTT with both reflections from MCS streamer data and refractions from OBS data, including arrivals revealed through DC. This approach better resolve the velocity structure of the shallow subsurface, reducing uncertainty in the sedimentary layer and consequently the position of the TOB. This mitigates the propagation of errors to deeper layers, leading to more accurate subsurface imaging.

- Building on our prior research on DC application to MCS data, this work introduces an additional effective solution by applying DC to WAS data. Through both studies and the corresponding DC software, we address the critical aspect of uncovering and identifying refractions regardless of the seismic dataset type. Notably, when MCS data is unavailable or unsuitable for redatuming, the DC approach remains a valid tool for processing WAS data alone or jointly with MCS, as shown in this work.

- Compared to regular TTT velocity models, DC-enhanced models provide a significant boost to the robustness of initial models used in FWI to achieve accurate high-resolution results. However, caution is necessary if the goal is applying these velocity models (from either TTT or FWI) for PSDM calculation. In scenarios with significant anisotropy and short streamer length relative to water depth, a combined model using MCS data for the shallow part of the model until the TOB and joint data for the deeper section is recommended for optimal PSDM results.

6 Code availability

The codes used in this study are available at GitHub repository under the GNU general public license v3.0:

- The new DC-WAS code: https://github.com/ejimeneztejero/DC_WAS.
- The 2D code version for traveltime tomography used to obtain the results in this study (https://github.com/ejimeneztejero/TOMO2D), and our 3D version (https://github.com/ejimeneztejero/TOMO3D_dev).

Acknowledgments

This is a contribution of the "Grup de Recerca Consolidat de la Generalitat de Catalunya" Barcelona Center for Subsurface Imaging (2017 SGR 1662). The work has been supported by project CONNECT with reference PID2021-128851OA-I00, ATLANTIS project (PID2019-109559RB- I00) and THREAT project (PID2021-128513OA-I00), funded by the Spanish Ministry of Science and Innovation. ICM has also had funding support of the 'Severo Ochoa Centre of Excellence' accreditation (CEX2019-000928-S), of the Spanish Research Agency (AEI). We acknowledge the use of the computational resources provided by CESGA (Galicia Supercomputing Center) for conducting the simulations reported in this paper.

References

[Arnulf et al. 2011] Arnulf, A. F., Singh, S. C., Harding, A. J., Kent, G. M., and Crawford, W. C.: Strong seismic heterogeneity in layer 2A near hydrothermal vents at the Mid-Atlantic Ridge, Geophys. Res. Lett., 38, L13320, https://doi.org/10.1029/2011GL047753, 2011.

[Arnulf et al. 2021] Arnulf, A.F., Biemiller, J., Lavier, L. et al. Physical conditions and frictional properties in the source region of a slow-slip event. Nat. Geosci. 14, 334–340 (2021). https://doi.org/10.1038/s41561-021-00741-0.

[Barison et al. 2011] Barison E., Brancatelli G., Nicolich R., Accaino F., Giustiniani M., Tinivella U.. "Wave equation datuming applied to marine OBS data and to land high resolution seismic profiling". Journal of Applied Geophysics, Volume 73, Issue 3, 2011, 267-277, ISSN 0926-9851, https://doi.org/10.1016/j.jappgeo.2011.01.009.

[Bartolome et al. 2004] Rafael Bartolome, Isabelle Contrucci, Hervé Nouzé, Emmanuelle Thiebot, Frauke Klingelhoëfer, Using the OBS wide-angle reflection/refraction velocities to perform a pre-stack depth migration image of the "single bubble" multichannel seismic: example of the Moroccan margin, Journal of Applied Geophysics, Volume 57, Issue 2, 2005, Pages 107-118, ISSN 0926-9851, https://doi.org/10.1016/j.jappgeo.2004.10.004.

[Begovic et al. 2017] Begovic, S., Melendez, A., Ranero, C. R., and Sallares, V.: Joint refraction and reflection travel-time tomography of multichannel and wide-angle seismic data, EGU General Assembly, Vienna, Austria, 23–28 April 2017, EGU2017-17231, 2017.

[Berkhout 1981] Berkhout, A. J.: Wavefield extrapolation techniques in seismic migration, a tutorial, Geophysics, 46, 1638–1656, https://doi.org/10.1190/1.1441172, 1981.

[Berkhout 1997a] Berkhout, A. J.: Pushing the limits of seismic imaging. Part I: prestack migration in terms of double dynamic focusing, Geophysics, 62(3), 937–953, https://doi.org/10.1190/1.1444201, 1997a.

[Berkhout 1997b] Berkhout, A. J.: Pushing the limits of seismic imaging. Part II: integration of prestack migration, velocity estimation, and AVO analysis, Geophysics, 62(3), 954–969, https://doi.org/10.1190/1.1444202, 1997b.

[Berryhill 1979] Berryhill, J. R.: Wave-equation datuming, Geophysics, 44, 13291344, https://doi.org/10.1190/1.1441010, 1979.

[Berryhill 1984] Berryhill, J. R.: Wave-equation datuming before stack, Geophysics, 49, 2064–2066, https://doi.org/10.1190/1.1441620, 1984.

[Bevc 1997] Bevc, D.: Flooding the topography: wave-equation datuming of land data with rugged acquisition topography, Geophysics, 62, 1558-1569, https://doi.org/10.1190/1.1885634, 1997.

[Cho et al. 2016] Cho, Y., Ha, W., Kim, Y., Shin, S., and Park, E.: Laplace-FourierDomain Full Waveform Inversion of Deep-Sea Seismic Data Acquired with Limited Offsets, Pure Appl. Geophys., 173, 749773, https://doi.org/10.1007/s00024-015-1125-7, 2016.

[Davy et al 2020] Davy, R. G., Collier, J. S., Henstock, T. J., & The VoiLA Consortium (2020). Wide-angle seismic imaging of two modes of crustal accretion in mature Atlantic Ocean crust. Journal of Geophysical Research: Solid Earth, 125, e2019JB019100. https://doi.org/10.1029/2019JB019100.

[Gazdag 1978] Gazdag, J.: Wave equation migration with the phase-shift method, Geophysics, 43, 13421351, https://doi.org/10.1190/1.1440899, 1978.

[Giustiniani et al. 2022] Giustiniani M., Tinivella U., Nicolich R., Chapter 8 - Imaging subsurface structures using wave equation datuming advanced seismic techniques, Editor(s): Rebecca Bell, David Iacopini, Mark Vardy, Interpreting Subsurface Seismic Data, Elsevier, 2022, Pages 199-234, ISBN 9780128185629, https://doi.org/10.1016/B978-0-12-818562-9.00004-2.

[Gras et al. 2019] Gras C., Dagnino D., Jiménez-Tejero C.E., Meléndez A., Sallarès V. and Ranero C.. Full-waveform inversion of short-offset, band-limited seismic data in the Alboran Basin (SE Iberia). Solid Earth, 10, 1833–1855, 2019 https://doi.org/10.5194/se-10-1833-2019.

[Grevemeyer et al 2018] Grevemeyer, I., Ranero, C.R., and Ivandic, M., Structure of oceanic crust and serpentinization at subduction trenches: Geosphere, doi:10.1130/GES01537.1. 2018.

[Jimenez-Tejero et al. 2022] Jimenez-Tejero C. E., Ranero C. R., Sallares V., Gras C., Downward continuation of marine seismic reflection data: an undervalued tool to improve velocity models, Geophysical Journal International, Volume 230, Issue 2, August 2022, Pages 831–848, https://doi.org/10.1093/gji/ggac087.

[Korenaga et al. 2000] Korenaga, J., Holbrook, W., Kent, G., Kelemen, P., Detrick, R., Larsen, H. C., et al. (2000). Crustal structure of the southeast Greenland margin from joint refraction and reflection seismic tomography. Journal of Geophysical Research, 105, 21591–21614. https://doi.org/10.1029/2000jb900188.

[Melendez et al. 2015a] Meléndez, A., Korenaga, J., and Miniussi, A.: Software TOMO3D, Barcelona Center for Subsurface Imaging, 2015a, available at: https://github.com/ejimeneztejero/TOMO3D_dev.

[Melendez et al. 2015b] Meléndez, A., Korenaga, J., Sallarès, V., Miniussi, A., and Ranero, C. R.: TOMO3D: 3-D joint refraction and reflection traveltime tomography parallel code for active-source seismic data – synthetic test, Geophys. J. Int., 203, 158–174, https://doi.org/10.1093/gji/ggv292, 2015b.

[Merino et al. 2021] I., Prada, M., Ranero, C. R., Sallares, V., Grevemeyer, I., Calahorrano, A., Cameselle, A.L. & Neres, M., 2021. The rift and continent-ocean transition structure under the Tagus Abyssal Plain West of the Iberia, J. geophys. Res., 126, e2021JB022629, doi:10.1029/2021JB022629.

[Mo 1997] Mo, L.: Datuming by wavefield extrapolation. Stanford Exploration Project, Report 75, 181-202: 1997.

[Moser 1991] Moser, T. J.: Shortest path calculation of seismic rays, Geophysics, 56, 59–67, https://doi.org/10.1190/1.1442958, 1991.

[Moser et al. 1992] Moser, T. J., Nolet, G., and Snieder, R.: Ray bending revisited, B. Seismol. Soc. Am., 82, 259–288, 1992.

[Olsen et al. 2020] Kelly M. Olsen, Nathan L. Bangs, Anne M. Tréhu, Shuoshuo Han, Adrien Arnulf, Eduardo Contreras-Reyes. Thick, strong sediment subduction along south-central Chile and its role in great earthquakes, Earth and Planetary Science Letters, Volume 538,2020,116195,ISSN 0012-821X,https://doi.org/10.1016/j.epsl.2020.116195.

[Reilly et al. 2019] O'Reilly B. M., Prada M., Lavoué F., Lebedev S., Predicting fluid pressure in sedimentary basins from seismic tomography, Geophysical Journal International, Volume 219, Issue 2, November 2019, Pages 1421–1430, https://doi.org/10.1093/gji/ggz378.

[Pasalic and McGarry 2010] D. Pasalic and R. McGarry, "Convolutional perfectly matched layer for isotropic and anisotropic acoustic wave equations," in Proc. SEG Tech. Program Expanded Abstracts, 2010, pp. 2925–2929.

[Peirce and Hobbs 2024] C Peirce, R W Hobbs, Oceanic crust—seismic structure, lithology and the cause of the 2A Event at borehole 504B, Geophysical Journal International, Volume 237, Issue 1, April 2024, Pages 159–189, https://doi.org/10.1093/gji/ggae029.

[Prada et al. 2019] Prada M., Lavoué F., Mudasar Saqab M. O'Reilly B., Lebedev S., Walsh J., Childs C. Across-axis variations in petrophysical properties of the North Porcupine Basin, offshore Ireland: New insights from long-streamer traveltime tomography. Volume31, Issue1, 2019, pages 59-76.

[Prada et al. 2023] Prada, M., Bartolomé, R., Gras, C. et al. Trench-parallel ridge subduction controls upper-plate structure and shallow megathrust seismogenesis along the Jalisco-Colima margin, Mexico. Commun Earth Environ 4, 53 (2023). https://doi.org/10.1038/s43247-023-00705-9

[Sallares and Ranero] Sallares V. & Ranero C.R., Depth-varying elastic properties of the upper plate determine mega-thrust earthquake rupture characteristics. Nature. https://doi.org/10.1038/s41586-019-1784-0 (2019).

[Sallares et al 2021] Sallares, V, Prada, M., Riquelme, S., Meléndez, A., Calahorrano, A., Grevemeyer, I. and Ranero, C. R., Large slip, long duration, and moderate shaking of the Nicaragua 1992 tsunami earthquake caused by low near-trench rock rigidity. Science Advances, 7 (32). eabg8659. DOI 10.1126/sciadv.abg8659. (2021).

[Shtivelman and Caning 1988] Shtivelman, V., and Caning, A.: Datum correction by wave-equation extrapolation, Geophysics, 53, 10, 1311–1322, https://doi.org/10.1190/1.1442409, 1988.

[Schuster and Zhou 2006] Schuster, G. T. and Zhou, M.: A theoretical overview of model based and correlation-based redatuming methods, Geophysics, 71, SI103–SI110, https://doi.org/10.1190/1.2208967, 2006.

[SU] Seismic Unix software. Software, manual and tutorial available at https://wiki.seismic-unix.org/. Software also available at https://github.com/JohnWStockwellJr/SeisUnix.

[Yang and Zhang 2019] Yang H. and Zhang J., "Reverse Time Migration of Refraction Waves in OBS Data," 2019 Photonics & Electromagnetics Research Symposium - Fall (PIERS - Fall), Xiamen, China, 2019, pp. 2812-2817, doi: 10.1109/PIERS-Fall48861.2019.9021637.

[Zhang and Shen 2010] W. Zhang and Y. Shen. Unsplit complex frequency-shifted PML implementation using auxiliary differential equations for seismic wave modeling. *Geophysics*, **75**, 4, 141-154. https://doi.org/10.1190/1.3463431.

[Zheng et al. 2019] Zheng, D., Herrmann, R.B. & He, X. Estimating Oceanic Crustal Structure from OBS Data Using Teleseismic P Wave Wavefield Continuation. Pure Appl. Geophys. 176, 4243–4259 (2019). https://doi.org/10.1007/s00024-019-02189-1.

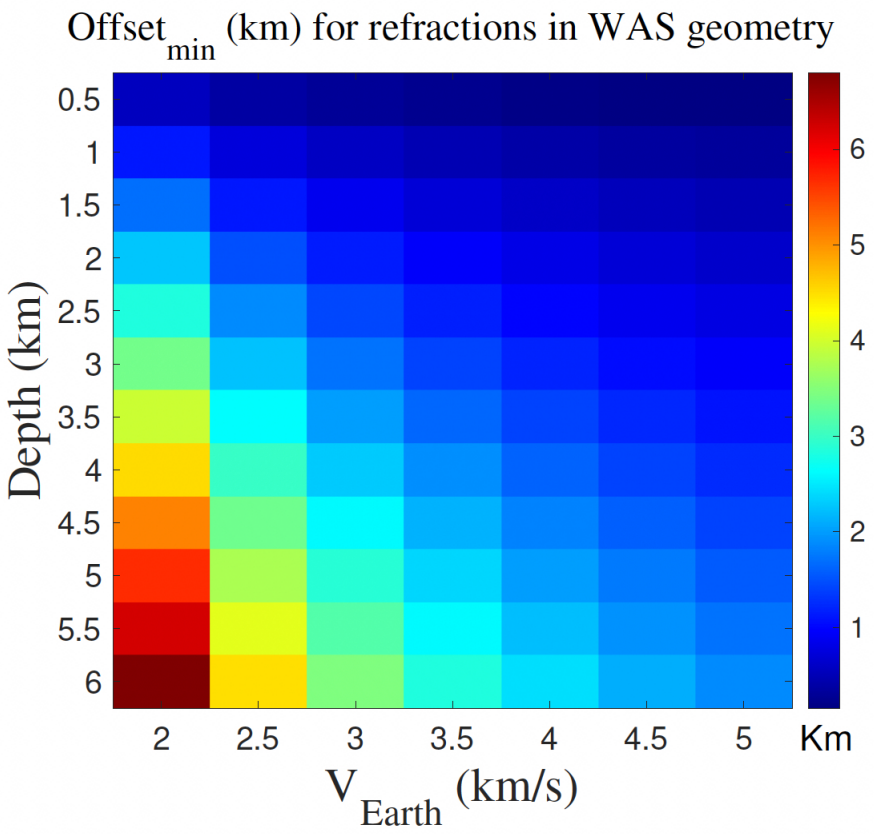

Figure 1: Minimum offset, as defined by Eq. 7 (for ϕ=0), represents the distance at which refractions are recorded in an OBS or OBH gather for a flat seafloor. The x-axis denotes the seafloor velocity parameter ranging from 2 to 5 km/s, while the y-axis represents the water column depth spanning from 0.5 to 6 km.

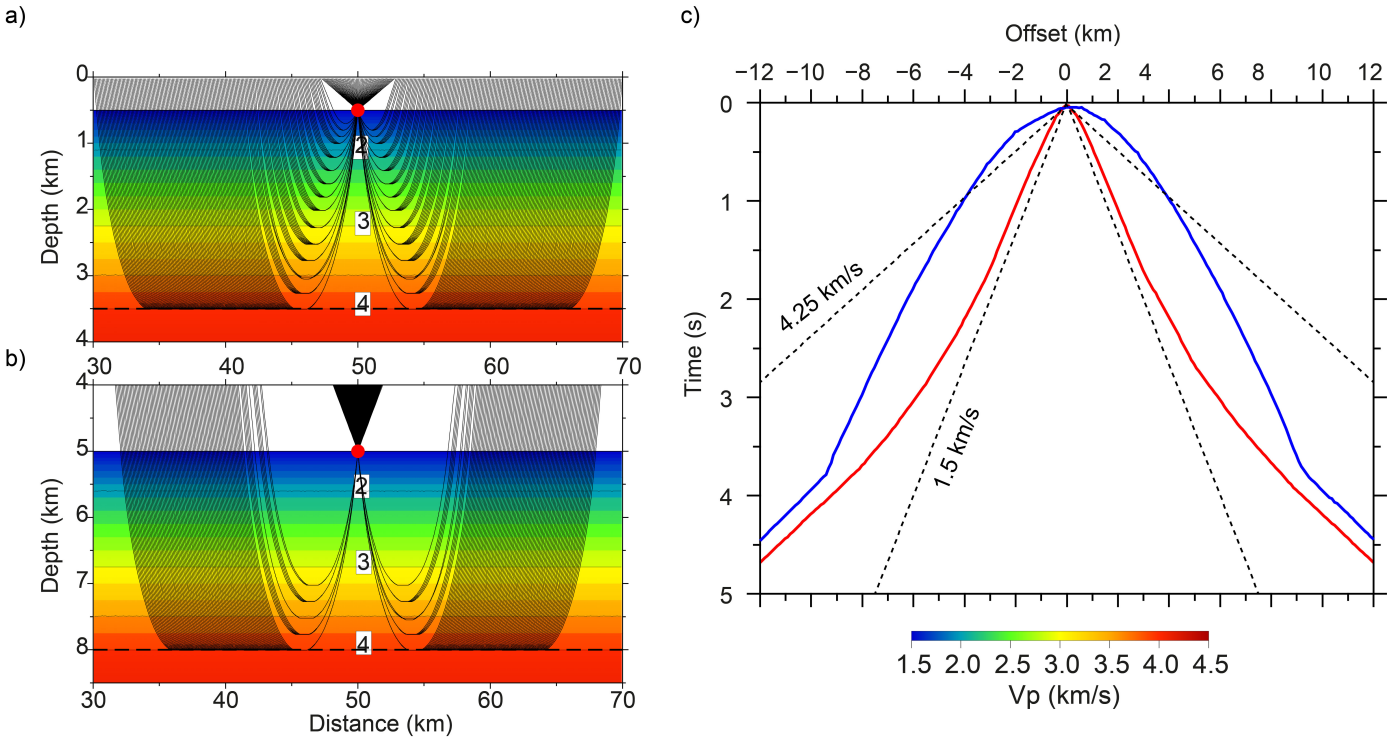

Figure 2: Panels a) and b) depict ray tracing simulations for varying water column depths: 0.5 km and 5 km, respectively. The velocity model applied in both panels features a 1D-gradient ranging from 1.5 to 4 km/s, extending from the seafloor to 3 km depth below it. In panel c), the first arrivals in the OBS gather are showcased with up to 12 km offset in both cases. The red line corresponds to the case presented in panel a) with a water depth of 0.5 km, while the blue line represents the scenario in panel b) with 5 km water depth.

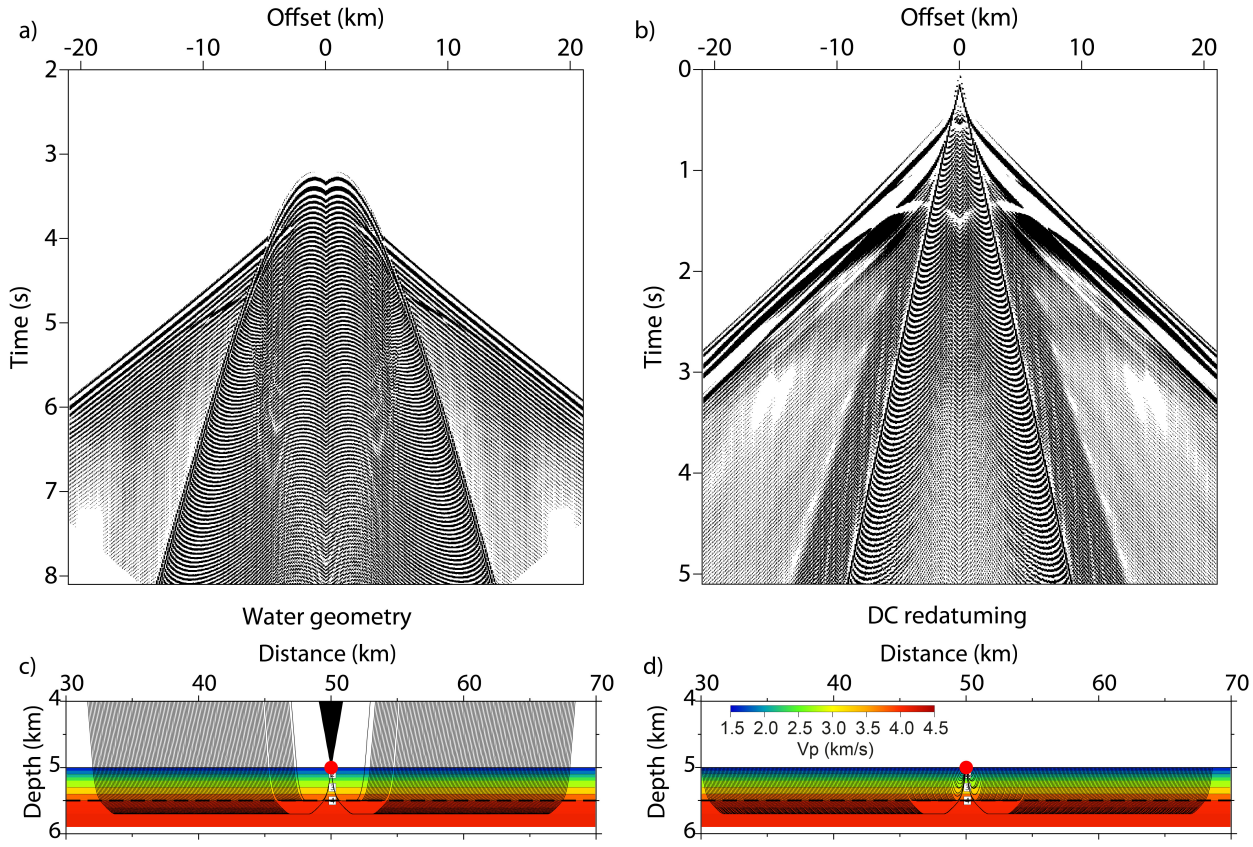

Figure 3: a) Synthetic OBS gather for a 1D-gradient model with a water depth of 5 km. b) Synthetic OBS gather after redatuming to the seafloor via DC. Panels c) and d) show ray tracing models corresponding to panels a) and b) respectively. First arrival refractions at offsets ¡ 8 km, mapping the shallow subseafloor structure, occur only in panel d).

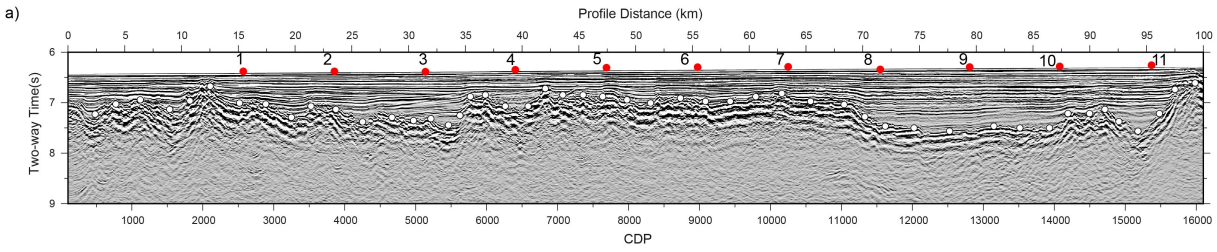

Figure 4: Seismic image of line ATLANTIS-I used in this work with the 11 OBH locations shown as red-filled circles dots. White dots delineate the TOB marking the contact between sediment cover and oceanic igneous crust. The map shows the location of the seismic line.

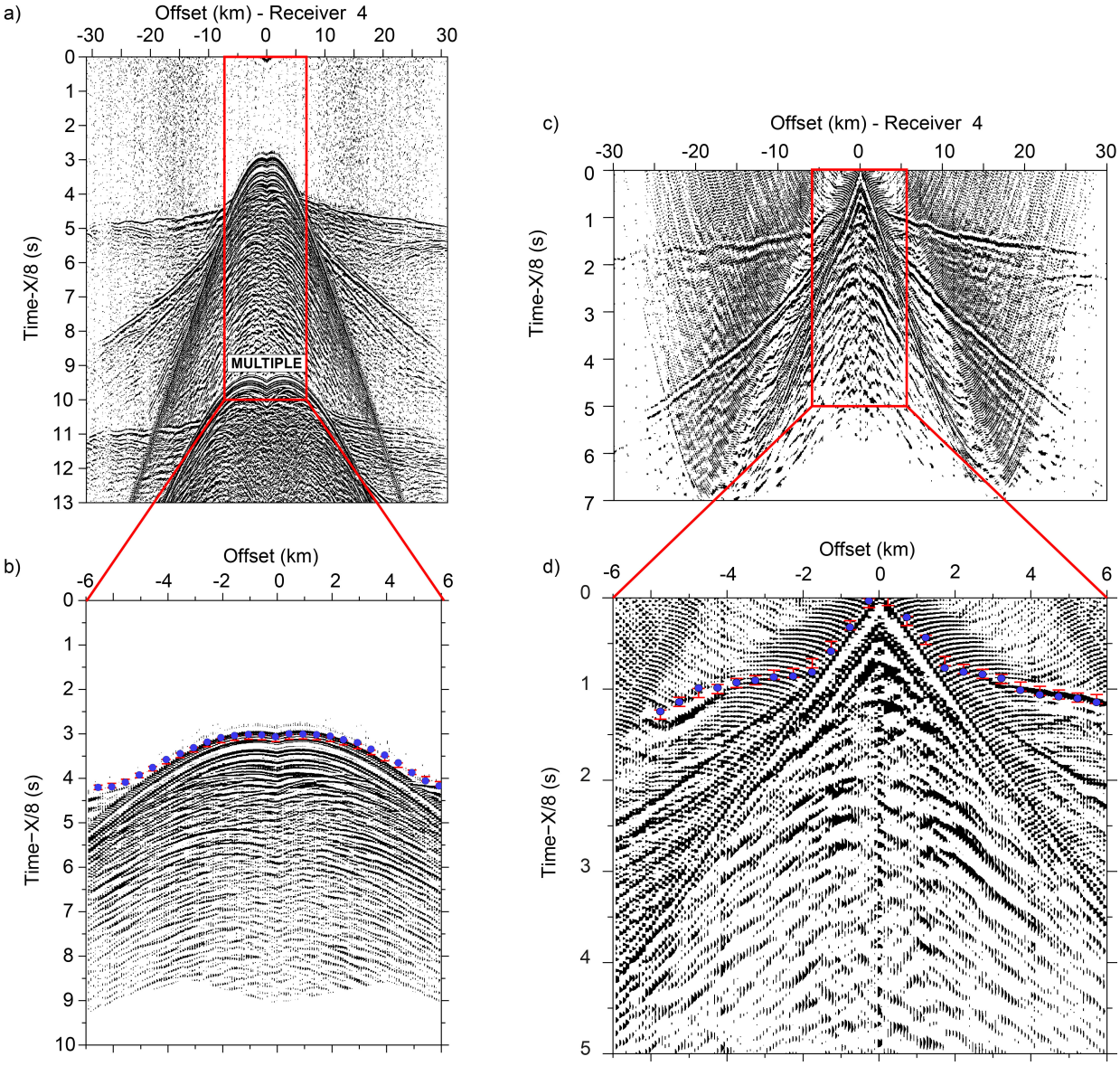

Figure 5: Taking OBH number 4 as an illustrative example, Panel a) presents the raw field data, while Panel b) offers a close-up view around 6 km offset, displaying the first arrival picks (blue dots) with the error bars (red bars). The same approach is employed in Panels c) and d), focusing on the OBH data downward continued to the seafloor.

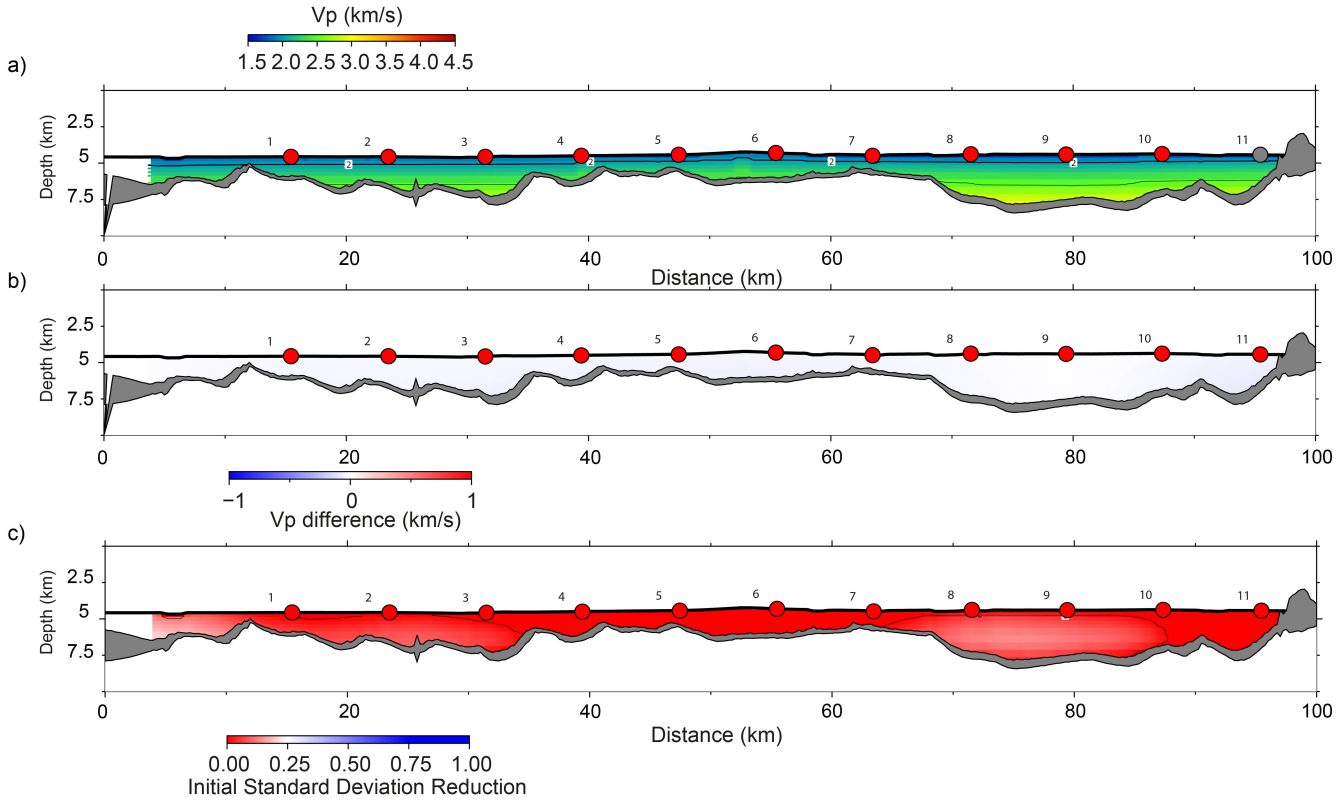

Figure 6: Results of travel-time tomography using only reflections recorded in MCS streamer data including V_p model and top of basement reflector geometry (grey horizon of variable thickness). a) Average V_p model derived from 500 realizations of the Montecarlo analysis. b) Disparity or misfit between the initial and average V_p model. c) Improvement in the initial standard deviation.

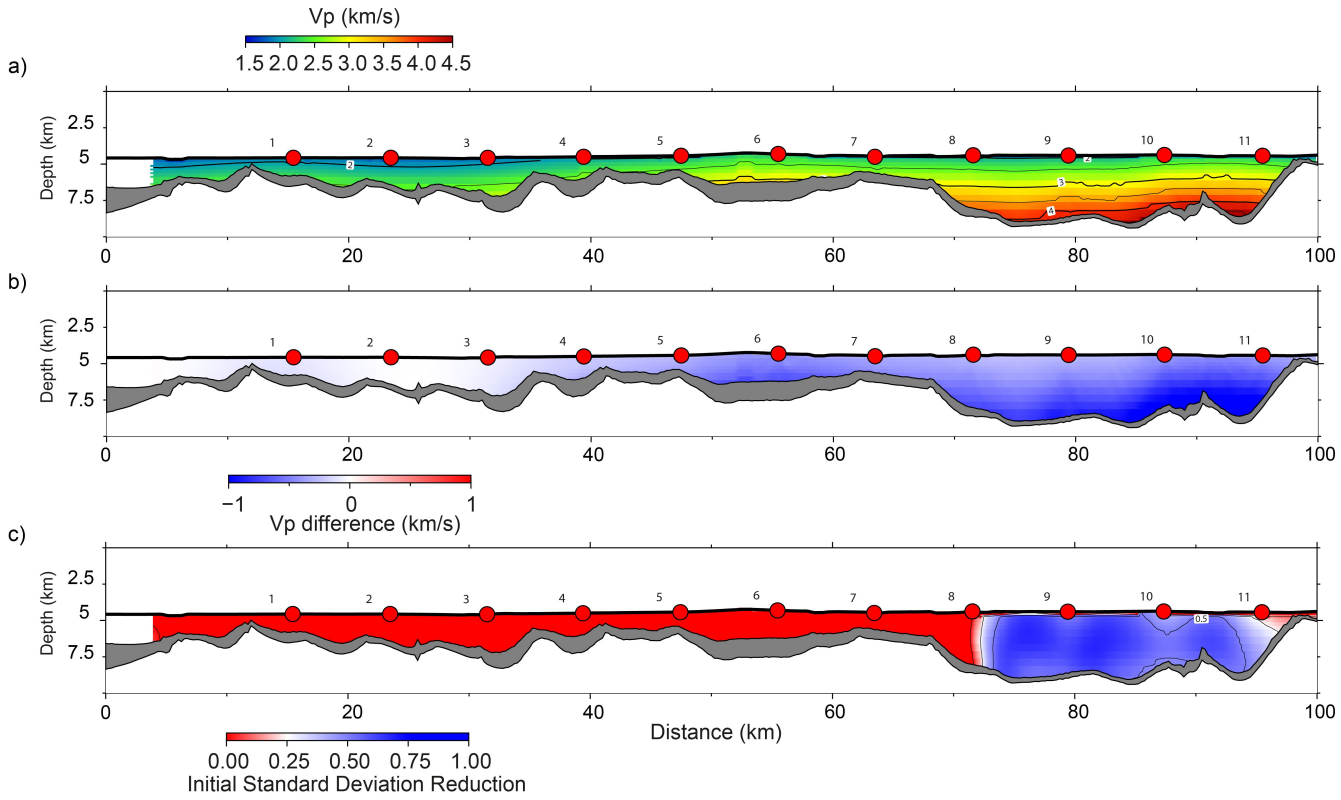

Figure 7: Results of travel-time tomography using reflections recorded in MCS streamer data and refractions in WAS data with standard geometry. The images include V_p model and top of basement reflector geometry (grey horizon of variable thickness). a) Average V_p model derived from 500 realizations of the Montecarlo analysis. b) Disparity or misfit between the initial and average V_p model. c) Improvement in the initial standard deviation.

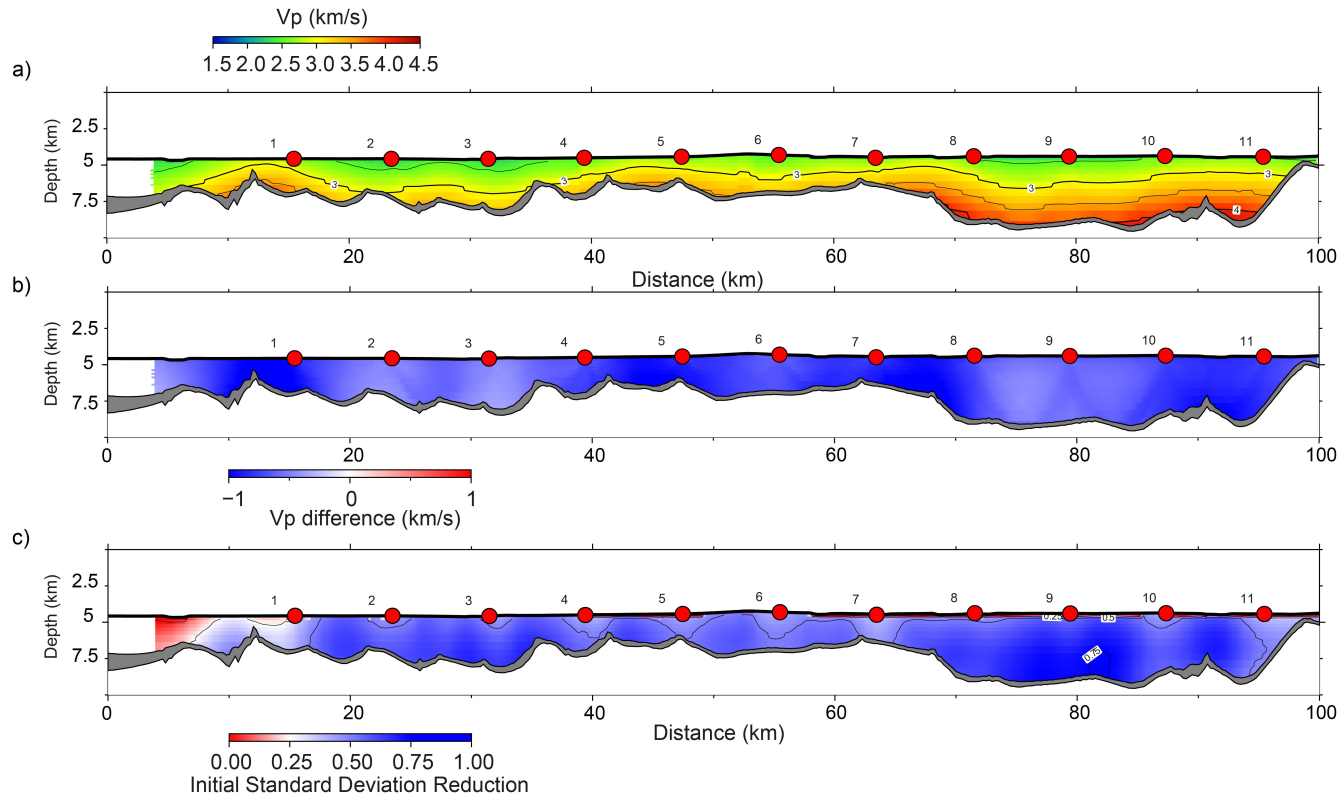

Figure 8: Results of travel-time tomography using reflections recorded in MCS streamer data and refractions in WAS data after DC redatuming. The images include V_p model and top of basement reflector geometry (grey horizon of variable thickness). a) Average V_p model derived from 500 realizations of the Montecarlo analysis. b) Disparity or misfit between the initial and average V_p model. c) Improvement in the initial standard deviation.

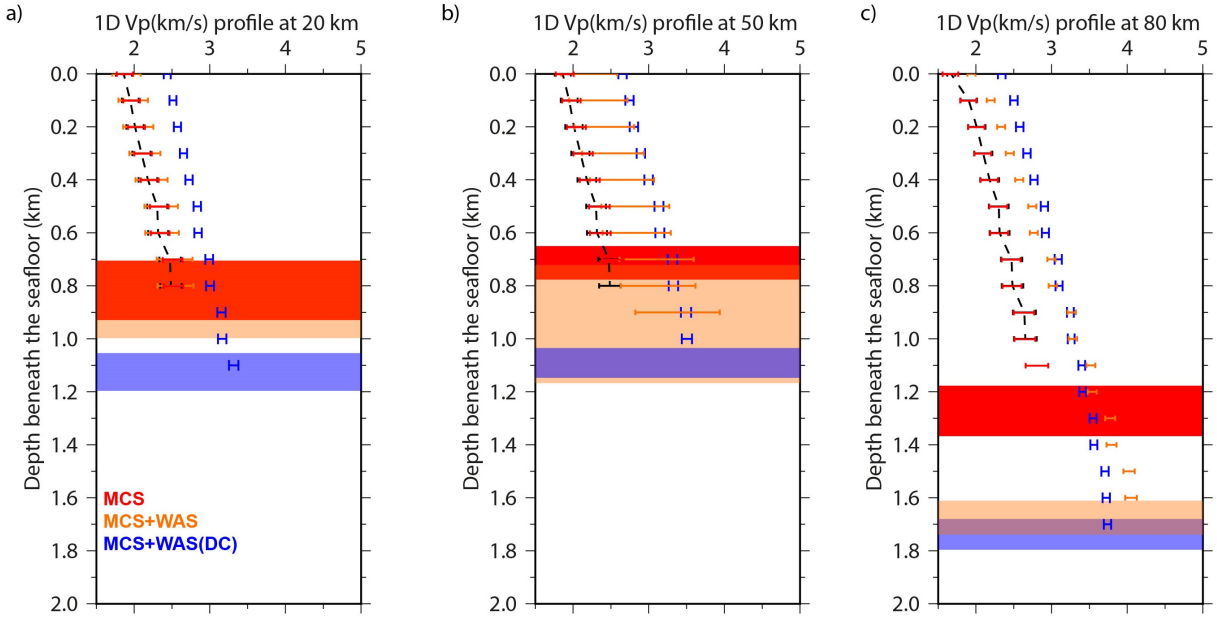

Figure 9: Comparison of the results of the three data sets inversion at km 20, 50, and 80 km along the seismic line. Color scheme refers to each strategy: red (MCS), orange (MCS+WAS), and purple (MCS+DC(WAS)). Error bars of 1D V_p indicate V_p uncertainty, and horizontal swath denote uncertainty in reflector locations

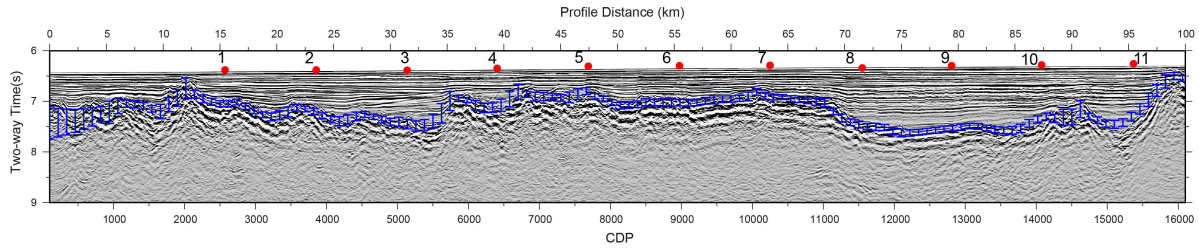

Figure 10: The analyzed seismic line presents the results of the TOB interpretation locations, accompanied by their respective error bars, in the context of using the joint strategy MCS + DC(WAS) case. OBH locations, numbered from 1 to 11, are denoted by red dots, and the TOB location results are illustrated with blue bars.

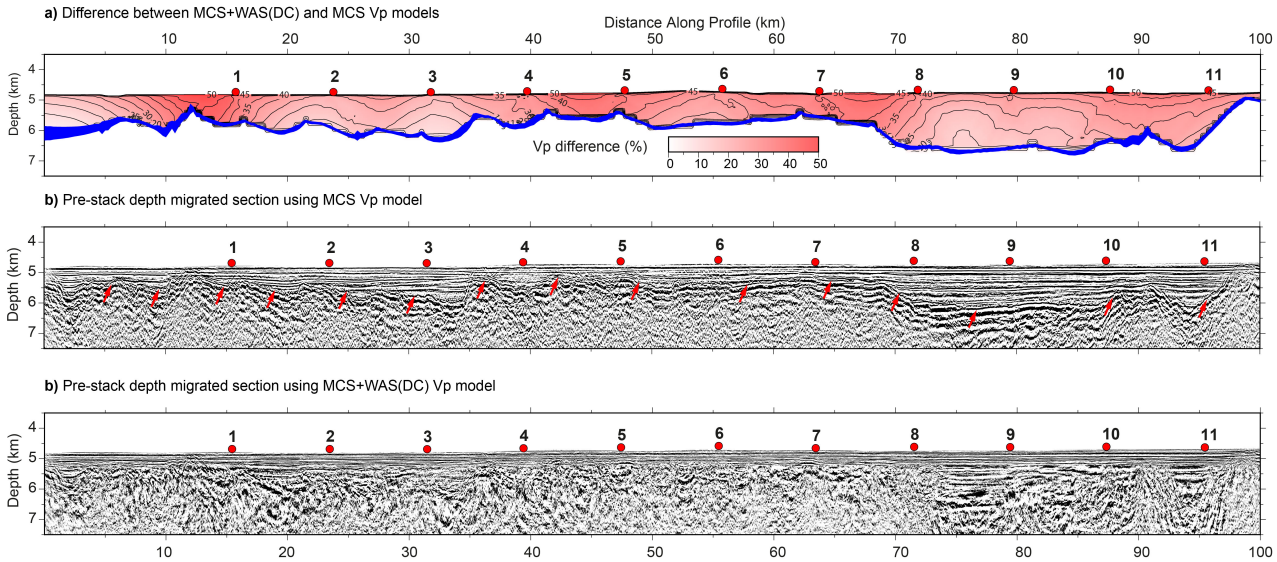

Figure 11: a) Difference between velocity models from MCS+WAS(DC) joint inversion and MCS data alone. On average, the velocity models differ by 18%. b) PSDM result using the combined approach, using the MCS velocity model for the shallow part until the TOB, and the DC-enhanced joint inversion velocity model, MCS+WAS(DC), for the deeper area. Red arrows indicate the TOB at various locations. c) PSDM result using the DC-enhanced joint inversion velocity model for the whole area, MCS+WAS(DC).

Supplementary Material

We provide supplementary material with three extra figures from the field data case analysis, as referenced in the study:

- Fig. S1: The rest of the OBS gathers used in the field data case study.
- Fig. S2: Initial Vp model and standard deviation used for the tomographic field data analysis and the final ones for each strategy: MCS, MCS+WAS, MCS+DC(WAS).
- Fig. S3: The comparison of the TOB reflector results across the entire seismic line, for each strategy: MCS, MCS+WAS, MCS+DC(WAS).

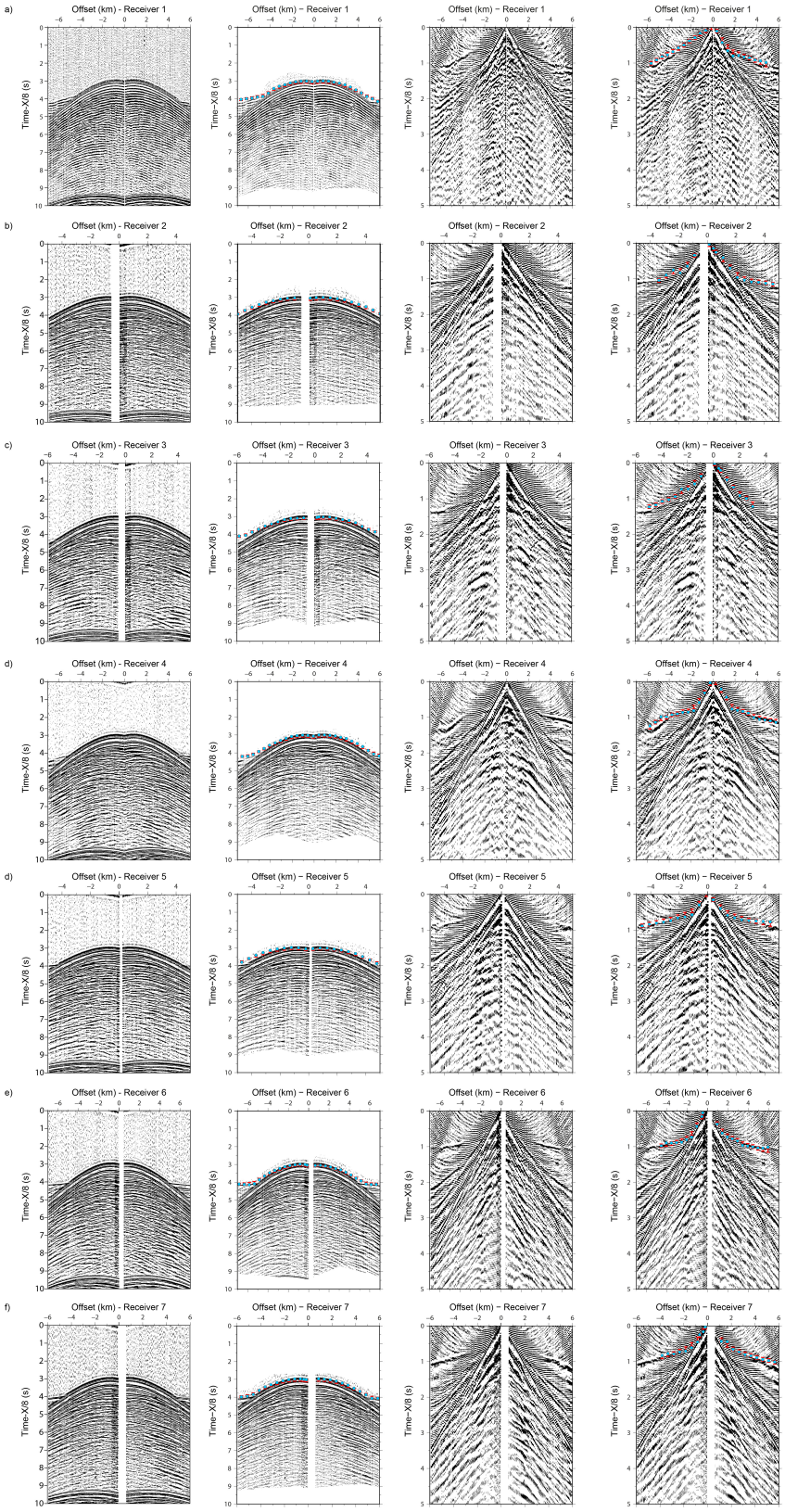

Figure S1: The rest of the OBS gathers used in the field data case study. The displayed data are organized into four columns for comparison. The first column depicts the raw OBS data. In the second column, OBS data are shown after muting prior to applying DC, where the mute of the signal is applied from time cero to the first arrival and from the first multiple to the end. The third column displays the result of redatuming the OBS data after applying DC. Finally, the fourth column mirrors the third but includes solid points in clue color indicating the first arrival and its corresponding error in red.

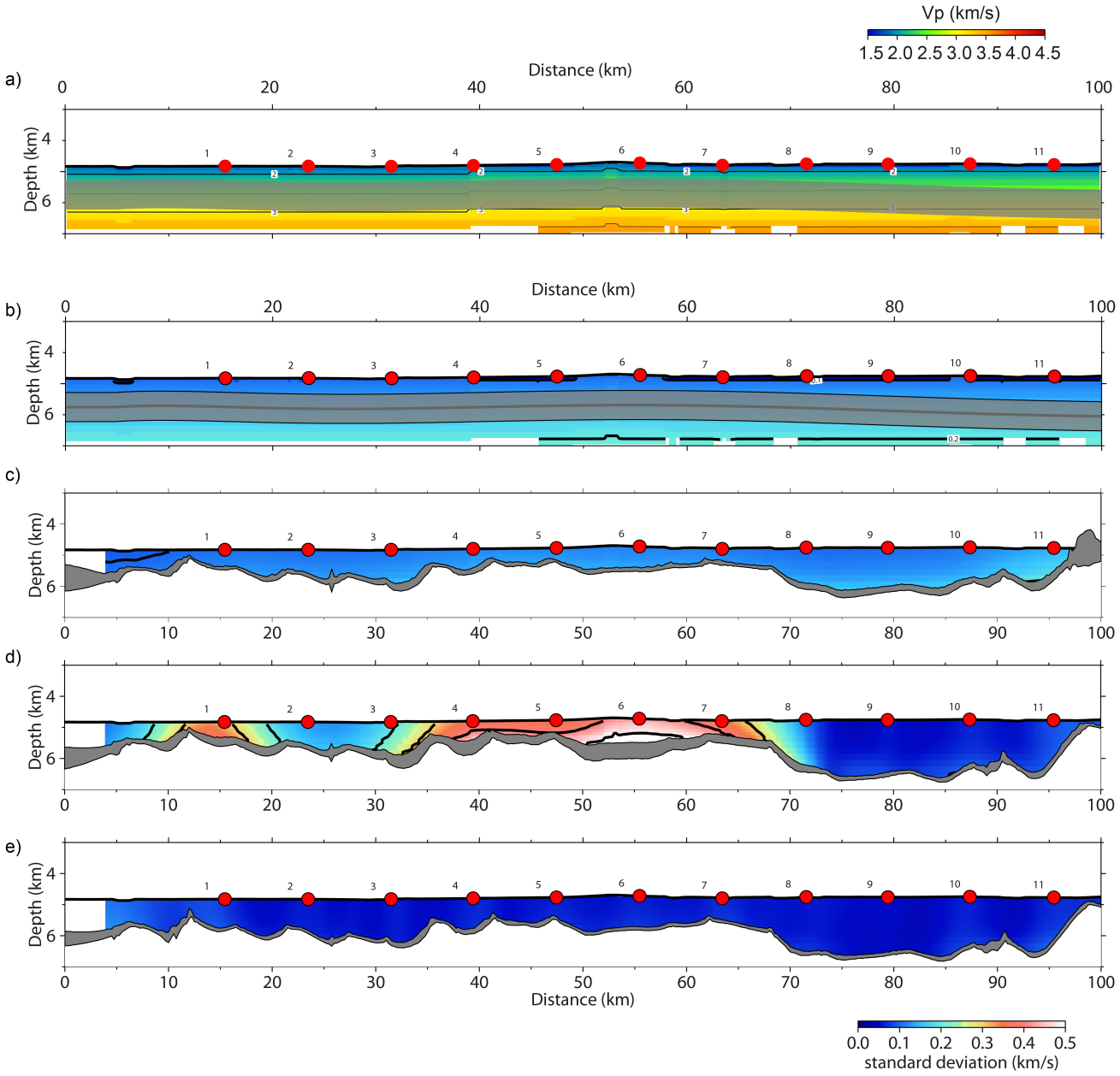

Figure S2: Initial Vp model and standard deviation used for the tomographic field data analysis and the final ones for each strategy: MCS, MCS+WAS, MCS+DC(WAS).

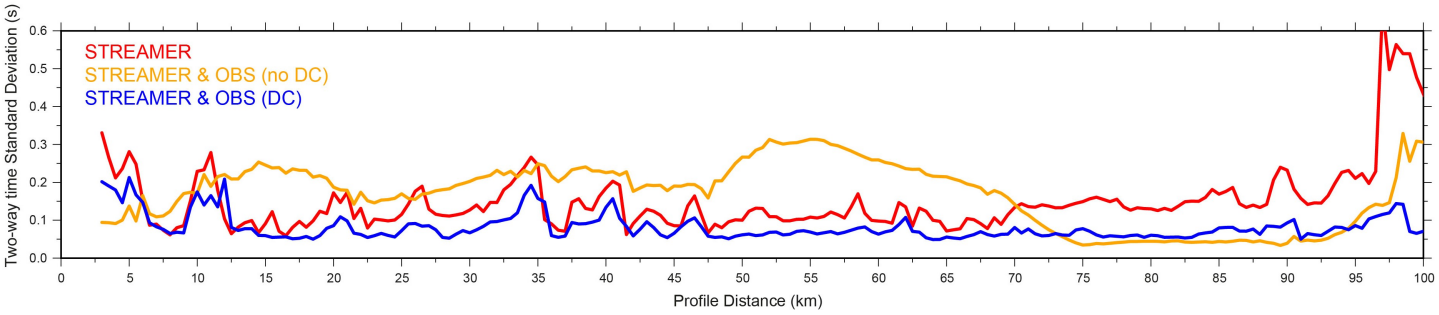

Figure S3: The TOB reflector results along the seismic line are compared for the three strategies analyzed: MCS represented by red, MCS+WAS by yellow and MCS+DC(WAS) by blue color-coding.